Energy-level statistics of interacting trapped bosons

Barnali Chakrabarti,[1,2] Anindya Biswas,[3] V. K. B. Kota,[4] Kamalika Roy,[2] and Sudip Kumar Haldar[2]
[1]*Instituto de Fisica, Universidade de São Paulo, Caixa Postale 66318, 05315-970 São Paulo, São Paulo, Brazil*
[2]*Department of Physics, Lady Brabourne College, P1/2 Suhrawardi Avenue, Kolkata 700017, India*
[3]*Department of Physics, University of Calcutta, 92 A.P.C. Road, Kolkata 700009, India*
[4]*Physical Research Laboratory, Navarangpura, Ahmedabad 380009, India*
(Received 15 May 2011; revised manuscript received 20 January 2012; published 23 July 2012)

It is a well-established fact that statistical properties of energy-level spectra are the most efficient tool to characterize nonintegrable quantum systems. The statistical behavior of different systems such as complex atoms, atomic nuclei, two-dimensional Hamiltonians, quantum billiards, and noninteracting many bosons has been studied. The study of statistical properties and spectral fluctuations in interacting many-boson systems has developed interest in this direction. We are especially interested in weakly interacting trapped bosons in the context of Bose-Einstein condensation (BEC) as the energy spectrum shows a transition from a collective nature to a single-particle nature with an increase in the number of levels. However this has received less attention as it is believed that the system may exhibit Poisson-like fluctuations due to the existence of an external harmonic trap. Here we compute numerically the energy levels of the zero-temperature many-boson systems which are weakly interacting through the van der Waals potential and are confined in the three-dimensional harmonic potential. We study the nearest-neighbor spacing distribution and the spectral rigidity by unfolding the spectrum. It is found that an increase in the number of energy levels for repulsive BEC induces a transition from a Wigner-like form displaying level repulsion to the Poisson distribution for $P(s)$. It does not follow the Gaussian orthogonal ensemble prediction. For repulsive interaction, the lower levels are correlated and manifest level-repulsion. For intermediate levels $P(s)$ shows mixed statistics, which clearly signifies the existence of two energy scales: external trap and interatomic interaction, whereas for very high levels the trapping potential dominates, generating a Poisson distribution. Comparison with mean-field results for lower levels are also presented. For attractive BEC near the critical point we observe the Shnirelman-like peak near $s = 0$, which signifies the presence of a large number of quasidegenerate states.

DOI: 10.1103/PhysRevA.86.013637 PACS number(s): 03.75.Hh, 05.45.Mt, 05.45.Pq

I. INTRODUCTION

Although there is no precise definition of the quantum chaos, the statistical properties of the energy-level spectra are often used to characterize level fluctuation in quantum systems. It is a well-established fact that for classically integrable systems the energy levels are uncorrelated and nearest-neighbor level spacing distribution ($P(s)$ distribution) follows Poisson statistics [1], whereas classically chaotic systems are associated with spectral fluctuations and strong level-repulsion between energy levels is described in random matrix theory [2–4]. $P(s)$ distribution follows the Gaussian orthogonal ensemble (GOE) or the Gaussian unitary ensemble (GUE) of random matrices depending on whether the Hamiltonian has time-reversal symmetry or not [2,4]. The spectral properties of many different many-fermion quantum systems like atoms and atomic nuclei and also quantum billiards have already been studied [3–11]. The $P(s)$ distribution of the nuclear data ensemble agrees very well with the GOE and in the atomic spectra the nearest-neighbor spacing distribution is of the Wigner type. In addition, recently there are some studies of spectral properties of noninteracting many-particle (fermions or bosons) systems [12] and interacting boson systems [10,11,13–15].

In the present work we undertake to study the quantum mechanical spectra, the statistical behavior of weakly interacting many-boson systems with an external harmonic confinement. This study is especially interesting for several reasons. First, it directly corresponds to the Bose-Einstein condensation (BEC) in dilute atomic vapor [16,17]. Second, due to the presence of external confinement the energy spectrum shows a transition from a collective nature to a single-particle nature [18,19]. Apparently it appears that the system will exhibit the most common Poisson statistics of integrable systems because at the near-zero temperature the interaction energy is small compared to the trap energy. However from earlier studies of different statistics and of thermodynamic and dynamic properties of the system, it is an established fact that interatomic interaction plays an important role even in the weakly interacting Bose gas [16–19]. Naturally this leads us to be more curious in the study of level spacing distribution. This is a different type of system where two energy scales coexist. One is the external trap which is characterized by the trap energy $\hbar\omega$ (ω is the external trap frequency). The other one is the interatomic interaction which is characterized by Na_s; where N is the number of bosons in the trap and the properties of zero-temperature BEC are essentially characterized by the s-wave scattering length a_s. Thus the study of spectral statistics of such a realistic system may provide exciting information on the level correlation and may disagree with the universal hypothesis of Bohigas, Giannoni, and Schmit [2]. Due to the existence of two energy scales, the system does obeys neither the regular Poisson distribution nor the GOE for a strongly chaotic system. We observe interesting features from the following study. Quantum mechanical spectra undergo a transition, as a function of a number of energy levels. It has already been observed both experimentally and theoretically that low-lying levels are strongly influenced by interatomic

interaction [18,19]. These levels are highly correlated and we observe the $P(s)$ distribution to be close to the Wigner distribution. The intermediate levels show a mixed statistics which is the overlap of both Poisson and Wigner distributions which clearly signifies the coexistence of two energy scales. Thus the choice in the number of levels has a great influence on the statistical properties. For higher levels (much above the chemical potential) the energy spectra are strictly dominated by the harmonic confinement and the energy levels are almost equidistant by the amount $\hbar\omega$, similar to the noninteracting harmonic oscillator, and this generates a Poisson distribution. To the best of our knowledge there are neither any systematic calculations nor any rigorous derivations in this direction. Here we tackle the problem by solving the trapped many-body system by using an *ab initio* but approximate many-body technique [20–22]. Because it is a complicated many-body problem, it is hard to present analytic studies. However our numerical study is also important because we investigate the statistical behavior of such a realistic condensate.

The paper is organized as follows. Section II deals with the many-body technique which basically calculates the many-body effective potential. The choice of interaction and the detailed calculation of energy levels are presented in Sec. III. Section IV deals with several statistical tools and numerical results. Section V concludes with a summary.

II. MANY-BODY TECHNIQUE

We start with the Hamiltonian of a $(N+1)$ trapped boson system written as [20,21]

$$H = -\frac{\hbar^2}{2m}\sum_{i=1}^{N+1}\nabla_i^2 + \sum_{i=1}^{N+1}V_{\rm trap}(\vec{x}_i) + \sum_{i,j=1,j<i}^{N+1}V(\vec{x}_i-\vec{x}_j), \tag{1}$$

where $V_{\rm trap}(\vec{x}_i)$ is the external trapping potential and $V(\vec{x}_i-\vec{x}_j)$ is the two-body pair interaction. We use the standard Jacobi coordinates defined as $\vec{\zeta}_i = (\frac{2i}{i+1})^{\frac{1}{2}}[\vec{x}_{i+1} - \frac{1}{i}\sum_{j=1}^{i}\vec{x}_j]$ $(i = 1,2,\ldots,N)$ and the center of mass through $\vec{R} = \frac{1}{N+1}\sum_{i=1}^{N+1}\vec{x}_i$. Then the relative motion of the atoms is described in terms of N Jacobi vectors $(\vec{\zeta}_1,\ldots,\vec{\zeta}_N)$ as [20,23]

$$\left[-\frac{\hbar^2}{m}\sum_{i=1}^{N}\nabla_{\zeta_i}^2 + V_{\rm trap} + V(\vec{\zeta}_1,\ldots,\vec{\zeta}_N) - E\right]\Psi(\vec{\zeta}_1,\ldots,\vec{\zeta}_N) = 0. \tag{2}$$

The hyperspherical harmonic expansion method (HHEM) is a convenient tool in many-body physics [23], where the expansion basis of the many-body wave function is the hyperspherical harmonics (HH). As the HH basis contains all possible correlations, its direct application to trapped bosons in the condensate which contains at least a few thousand bosons is an impossible task. Very recently we have adopted a technique called the potential harmonic expansion method (PHEM) which keeps all possible two-body correlations together with realistic interatomic interaction [20,22]. For the dilute Bose gas, the effect of two-body correlations is important and one can safely ignore the effect of all higher-body correlations. That is, when two atoms interact the rest bosons are inert spectators and for zero-temperature BEC this is a justified approximation. Thus for the spinless bosons, we decompose Ψ in two-body Faddeev components:

$$\Psi = \sum_{ij>i}^{N+1}\psi_{ij}. \tag{3}$$

Hence ψ_{ij} is a function of a two-body separation vector only, besides the global length (hyperradius, see below). ψ_{ij} (symmetric under P_{ij}) satisfies the Schrödinger equation

$$(T - E + V_{\rm trap})\psi_{ij} = -V(\vec{x}_{ij})\sum_{k,l>k}\psi_{kl}, \tag{4}$$

T being the total kinetic energy; operating $\sum_{i,j>i}$ on both sides of Eq. (4) we get back the original Schrödinger equation. The hyperradius is defined as $r = \sqrt{\sum_{i=1}^{N}\zeta_i^2}$. The hyperradius and $(3N-1)$ hyperangles (denoted by Ω_N) together constitute $3N$ hyperspherical variables. The choice of Jacobi coordinates is not fixed as the labeling of the particle indices is arbitrary. We choose a particular set for the (ij) interacting pair, called the (ij) partition, by taking $\vec{r}_{ij}$ as $\vec{\zeta}_N$, and (ϑ,φ) are two spherical polar angles of the separation vector $\vec{r}_{ij}$. The angle ϕ is defined by $r_{ij} = r\cos\phi$. For the remaining $(N-1)$ Jacobi coordinates we define the hyperradius for the partition (ij) as $\rho_{ij} = [\sum_{k=1}^{N-1}\zeta_k^2]^{\frac{1}{2}}$ such that $\rho_{ij}^2 + r_{ij}^2 = r^2$ and $\rho_{ij} = r\sin\phi$. With this choice, the hyperspherical coordinates are

$$(r,\Omega_N) = (r,\phi,\vartheta,\varphi,\Omega_{N-1}), \tag{5}$$

where Ω_{N-1} involves $(3N-4)$ variables: $2(N-1)$ polar angles associated with $(N-1)$ Jacobi vectors $\vec{\zeta}_1,\ldots,\vec{\zeta}_{N-1}$ and $(N-2)$ angles defining the relative lengths of these Jacobi vectors [23]. Then the Laplacian in $3N$-dimensional space has the form

$$\nabla^2 \equiv \sum_{i=1}^{N}\nabla_{\zeta_i}^2 = \frac{\partial^2}{\partial r^2} + \frac{3N-1}{r}\frac{\partial}{\partial r} + \frac{L^2(\Omega_N)}{r^2}, \tag{6}$$

where $L^2(\Omega_N)$ is the grand orbital operator in $D = 3N$ dimensional space. Potential harmonics for the (ij) partition are defined as the eigenfunctions of $L^2(\Omega_N)$ corresponding to the zero eigenvalue of $L^2(\Omega_{N-1})$. The corresponding eigenvalue equation satisfied by $L^2(\Omega_N)$ is [23]

$$[L^2(\Omega_N) + \mathcal{L}(\mathcal{L}+D-2)]\mathcal{P}_{2K+l}^{l,m}(\Omega_{ij}) = 0, \qquad \mathcal{L} = 2K + l\cdot \tag{7}$$

This new basis is a subset of the HH basis and is called the potential harmonics (PH) basis. It does not contain any function of the coordinate $\vec{\zeta}_i$ with $i < N$ and is given by [23]

$$\mathcal{P}_{2K+l}^{l,m}(\Omega_{(ij)}) = Y_{lm}(\omega_{ij})\,{}^{(N)}P_{2K+l}^{l,0}(\phi)\mathcal{Y}_0(D-3), \tag{8}$$

where $Y_{lm}(\omega_{ij})$ is the spherical harmonics and $\omega_{ij} = (\vartheta,\varphi)$. The function ${}^{(N)}P_{2K+l}^{l,0}(\phi)$ is expressed in terms of Jacobi polynomials and $\mathcal{Y}_0(3N-3)$ is the HH of order 0 in the $(3N-3)$-dimensional space, spanned by $\{\vec{\zeta}_1,\ldots,\vec{\zeta}_{N-1}\}$ Jacobi vectors [23]. Thus the contribution to the grand orbital quantum number comes only from the interacting pair and the $3N$-dimensional Schrödinger equation reduces effectively to a four-dimensional equation. The relevant set of quantum numbers is the following: orbital l, azimuthal m, and grand

orbital $2K + l$ for any N. The full set of quantum numbers is

$$l_1 = l_2 = \cdots = l_{N-1} = 0, \quad l_N = l \tag{9}$$
$$m_1 = m_2 = \cdots = m_{N-1} = 0, \quad m_N = m \tag{10}$$
$$n_2 = n_3 = \cdots = n_{N-1} = 0, \quad n_N = K. \tag{11}$$

We expand the (ij)-Faddeev component, ψ_{ij}, in the complete set of the PH basis appropriate for the (ij) partition:

$$\psi_{ij} = r^{-(\frac{3N-1}{2})} \sum_K \mathcal{P}^{lm}_{2K+l}\left(\Omega_N^{(ij)}\right) u^l_K(r), \tag{12}$$

which includes only two-body correlations. Substituting it in Eq. (4) and projecting on a particular PH, a set of coupled differential equations (CDE) is obtained [20,21]:

$$\left[-\frac{\hbar^2}{m}\frac{d^2}{dr^2} + \frac{\hbar^2}{mr^2}\{\mathcal{L}(\mathcal{L}+1) + 4K(K+\alpha+\beta+1)\} - E + V_{\rm trap}(r)\right] U_{Kl}(r) + \sum_{K'} f_{Kl} V_{KK'}(r) f_{K'l} U_{K'l}(r) = 0, \tag{13}$$

with $U_{Kl}(r) = f_{Kl} u^l_K(r)$, $\mathcal{L} = l + \frac{3N-3}{2}$, $\alpha = \frac{3N-8}{2}$, $\beta = l + \frac{1}{2}$, l being the orbital angular momentum contributed by the interacting pair, and K being the hyperangular momentum quantum number. f_{Kl} is a constant representing the overlap of the PH for the interacting partition with the full set, which is given in Ref. [20]. The potential matrix element $V_{KK'}(r)$ is given by [20]

$$V_{KK'}(r) = \int \mathcal{P}^{lm^*}_{2K+l}\left(\Omega_N^{ij}\right) V(x_{ij}) \mathcal{P}^{lm}_{2K'+l}\left(\Omega_N^{ij}\right) d\Omega_N^{ij}. \tag{14}$$

So far we have disregarded the effect of the strong short-range correlation in the PH basis. In the experimental BEC, the average interparticle separation is much larger than the range of two-body interaction. This is indeed required to prevent atomic three-body collisions and formation of molecules. As the energy of the interacting pair is extremely small, the two-body interaction is generally represented by the s-wave scattering length (a_s). A positive value of a_s gives a repulsive condensate and a negative value of a_s gives an attractive condensate. However a realistic interaction, like the van der Waals potential, is always associated with an attractive $-\frac{1}{x_{ij}^6}$ tail at larger separation and a strong repulsion at short separation. Depending on the nature of these two parts, a_s can be either positive or negative. For a given finite-range, the two-body potential a_s can be obtained by solving the zero-energy two-body Schrödinger equation for the wave function $\eta(x_{ij})$:

$$-\frac{\hbar^2}{m}\frac{1}{x_{ij}^2}\frac{d}{dx_{ij}}\left(x_{ij}^2\frac{d\eta(x_{ij})}{dx_{ij}}\right) + V(x_{ij})\eta(x_{ij}) = 0. \tag{15}$$

The correlation function quickly attains its asymptotic form $C(1 - \frac{a_s}{x_{ij}})$ for large x_{ij}. The asymptotic normalization is chosen to make the wave function positive at large x_{ij} [22]. In the experimental BEC, the energy of the interacting pair is negligible compared with the depth of the interaction potential. Thus $\eta(x_{ij})$ is a good approximation of the short-range behavior of ψ_{ij}. Then we introduce this correlation function in the expansion basis and call it the correlated potential harmonics (CPH) basis:

$$\left[\mathcal{P}^{l,m}_{2K+l}(\Omega_{(ij)})\right]_{\rm corr} = Y_{lm}(\omega_{ij})\, {}^{(N)}P^{l,0}_{2K+l}(\phi)\mathcal{Y}_0(3N-3)\eta(x_{ij}), \tag{16}$$

where $\eta(x_{ij})$ correctly reproduces the short separation behavior of the interacting-pair Faddeev component. The convergence rate of the PH expansion is quite fast. The correlated potential matrix element $V_{KK'}(r)$ is now given by

$$V_{KK'}(r) = \left(h^{\alpha\beta}_K h^{\alpha\beta}_{K'}\right)^{-\frac{1}{2}} \int_{-1}^{+1} \left\{ P^{\alpha\beta}_K(z) V\left(r\sqrt{\frac{1+z}{2}}\right) \times P^{\alpha\beta}_{K'}(z)\eta\left(r\sqrt{\frac{1+z}{2}}\right) w_l(z)\right\} dz. \tag{17}$$

Here $h^{\alpha\beta}_K$ and $w_l(z)$ are, respectively, the norm and the weight function of the Jacobi polynomial $P^{\alpha\beta}_K(z)$ [20,21]. K and K' are the grand orbital quantum numbers of the basis sets in which the potential matrix is calculated.

III. CHOICE OF INTERACTION AND CALCULATION OF ENERGY LEVELS

For the present study we consider a few thousand (1000–10000) ^{87}Rb atoms in the JILA trap [16,17]. Throughout our calculation we choose $a_{ho} = \sqrt{\frac{\hbar}{m\omega}}$ as the unit of length (oscillator unit) and energy is expressed in units of the oscillator energy ($\hbar\omega$). The van der Waals potential has been chosen as the interatomic potential with a hard core of radius r_c, viz., $V(x_{ij}) = \infty$ for $x_{ij} \leqslant r_c$ and $-\frac{C_6}{x_{ij}^6}$ for $x_{ij} > r_c$. The strength C_6 is taken as 6.4898×10^{-11} o.u. for ^{87}Rb atoms in the JILA experiment [17]. We adjust the cutoff radius r_c in the two-body equation to correctly obtain $a_s = 2.09 \times 10^{-4}$ o.u.

With these sets of parameters we solve the set of coupled differential equations [Eq. (13)] by the hyperspherical adiabatic approximation (HAA) [24]. We assume that the hyperadial motion is slow in comparison with the hyperangular motion. For the hyperangular motion for a fixed value of r, we diagonalize the potential matrix together with the hypercentrifugal term. Thus for a fixed value of r, the equation for the hyperangular motion can be solved adiabatically. The eigenvalue of this equation is a parametric function of r and provides an effective potential for the hyperradial motion. In the HAA, the lowest eigenpotential is used for the ground state of the system and the hyperangular motion appears through the coupling matrix $V_{KK'}(r)$. Thus the whole condensate collectively oscillates in the effective potential. The energy is thus obtained by solving the equation for the hyperradial motion as [24]

$$\left[-\frac{\hbar^2}{m}\frac{d^2}{dr^2} + \omega_0(r) + \sum_{K=0}^{K_{\rm max}} \left|\frac{d\chi_{K0}(r)}{dr}\right|^2 - E\right]\zeta_0(r) = 0, \tag{18}$$

subject to the appropriate boundary conditions on $\zeta_0(r)$. This is called the uncoupled adiabatic approximation (UAA), whereas disregarding the third term corresponds to the extreme adiabatic approximation. The HAA has already been successfully applied in different atomic and nuclear cases.

Although the lower multipolarities have been successfully detected in the experiments [18], the collective excitations with higher multipolarity are also important especially to study the thermodynamic properties [19]. In our many-body picture, the collective motion of the condensate is characterized by the effective potential as described earlier. Thus the excited states in this potential are the states with the lth surface mode and the nth radial excitation, which are denoted by E_{nl}. Thus $n = 0$ and $l = 0$ correspond to the ground state and for $l \neq 0$ we get the surface modes. To calculate the higher levels with $l \neq 0$ we follow the next procedure. For $l \neq 0$, a large inaccuracy is involved in the calculation of the off-diagonal potential matrix and numerical computation becomes very slow. However, the main contribution to the potential matrix comes from the diagonal hypercentrifugal term and we disregard the off-diagonal matrix element for $l > 0$. Thus we get the effective potential $\omega_l(r)$ in the hyperradial space for $l \neq 0$. The energy of the lowest modes is in close agreement with the other calculations [18,19,25,26] and we observe that, for energy much larger than the chemical potential, the excited states are separated at energy close to the harmonic energy $\hbar\omega$ as in the noninteracting harmonic oscillator model. This transition from the low-energy collective to the high-energy single-particle spectrum leads us to study further the level fluctuation and other statistical behavior.

Before discussing the statistical behavior of the energy spectrum we discuss how good our approximation method is. There are many approximation methods to calculate the low-lying collective excitations and also the higher multipolarities. All these basically use the uncorrelated mean-field theory and the hydrodynamic method. The hydrodynamic method is good for a large number of bosons in the trap in the Thomas-Fermi limit, whereas our system is finite sized and has a few thousand bosons. As the system is not exactly solvable like the one-dimensional system with contact δ interaction, it is not possible to calculate the accuracy of our approximation method. However, from our previous calculations of different measurable quantities like the critical instability of attractive BEC, the collective excitations, and the thermodynamic properties, we observed that the correlated PHEM is an improvement over the Gross-Pitaevskii (GP) mean-field treatment for several reasons. Although the GP mean-field equation is widely used, the wave function does not include any correlation. It is pointed out by several authors that the replacement of the actual interaction by a contact potential is not appropriate for a general realistic potential which consists of a repulsive core and an attractive part [27–29]. The earlier studies also indicate the necessity of shape-dependent potentials instead of the zero-range potential [30,31]. The choice of contact interaction especially for three-dimensional attractive BEC is not satisfactory [30] as the δ-function interaction produces an essential singularity at $r = 0$. Thus to include correlations, one must go beyond the mean-field approximations and use the finite-range realistic potentials. Thus the correlated potential harmonics basis and the PHEM are a step in the right direction. This basis set retains all two-body correlations and assumes that three- and higher-body correlations are negligible. For dilute condensate it is perfectly justified. However including all two-body correlations we go beyond the mean-field theory. As the number of variables is reduced to only *four* for any number of bosons in the trap, we can treat quite a large number of atoms in the trap without much numerical complication. The use of a van der Waals potential having a finite range takes care of the short-range repulsion and interatomic correlations. Clearly it is an improvement over the GP mean-field theory.

The correlated many-body approach has been successfully applied in the calculation of static properties in different traps, collective excitations, and thermodynamic properties of trapped bosons [20–22,25,26,32–35]. In Refs. [25,26], we have calculated the low-lying collective excitations by the PHEM both for repulsive and attractive BEC. It has been shown that for repulsive and weak interaction the many-body results are close to the numerical solution of the GP equation. However for large repulsive interaction a significant difference is found. For the attractive BEC, the excitation frequencies for low-lying modes are well comparable with the self-consistent Popov approximation. However higher multipolarities are lower than the GP result. This is attributed to the two-body correlations and finite-range interaction of the realistic interatomic interaction. In Ref. [32], the PHEM is extended to investigate thermodynamic quantities which involves the calculation of a large number of energy levels. The calculated critical temperature and the condensate fraction have been calculated and compared with the GP results. The effects of realistic interatomic interactions and two-body correlations on thermodynamic properties of trapped bosons are observed. Thus the calculated energy levels are accurate for further analysis. We check for the convergence such that the error is considerably smaller than the mean level spacing.

Now to corroborate with the experiments we need the following discussions. Exciting the condensate by applying inhomogeneous oscillatory force with tunable frequency, it is possible to observe several modes with different angular momentum and energy in the collective excitations [18]. These experiments mainly concern low-lying collective excitations where the effect of interatomic interaction is prominant and the high-lying spectra should exhibit the single-particle nature. The transition from collective to single-particle excitations has also been studied in detail theoretically [19]. The collective excitations have also dramatic dependence on the temperature which comes from the interaction between the condensate and the thermal cloud [36,37]. But for the present study we consider the zero-temperature BEC and the effect of thermal fluctuations does not arise. There is no damping in the condensate as we assume there are no thermally excited atoms. Apparently this may contradict the experimental situation. But in the presence of external trapping and at zero temperature the effect of damping is not critical.

IV. STATISTICAL TOOLS AND NUMERICAL RESULTS

After getting the many-body collective levels including higher-order excitations with different l, we transform the spectrum. Next to characterize the spectral fluctuation in the many-body energy spectrum and to compare the statistical properties of different parts of the spectrum we remove the smooth part in the level density. In general, the level density has two parts: one is the smooth part which defines the general trend of the energy spectrum and the other is a fluctuating part. The smooth part is removed by unfolding

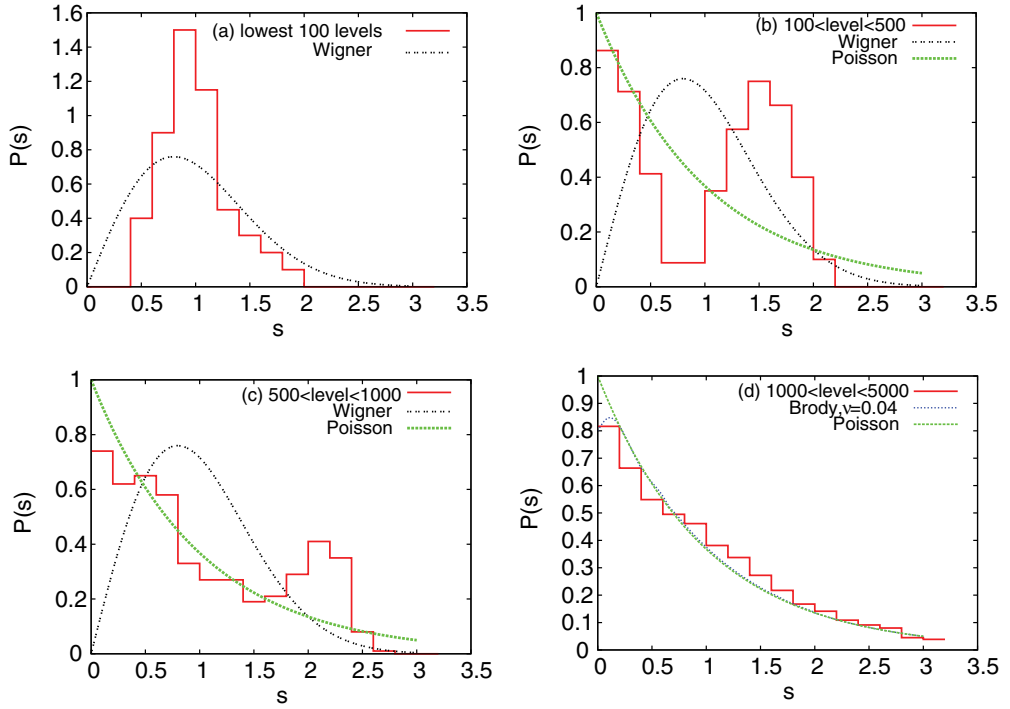

FIG. 1. (Color online) The $P(s)$ distribution is presented for different numbers of levels as indicated in the panels: (a) Lowest 100 levels, (b) 100 to 500 levels, (c) 500 to 1000 levels, and (d) 1000 to 5000 levels. In each panel the histogram presents the $P(s)$ distribution for the Hamiltonian (1) with $N = 1000$ interacting bosons. The black dotted curve represents the Wigner distribution [panels (a)–(c)] and the green dashed curve represents the Poisson distribution [panels (b)–(d)]. The blue dotted curve in panel (d) corresponds to the Brody distribution, with the corresponding Brody parameter being $\nu = 0.04$.

which maps the energy levels to another with the mean level density equal to 1. Several unfolding procedures are described in Refs. [4,38]. For the present calculation the many-body level density is approximated by a polynomial and unfolding is done by a seventh-order polynomial. We unfold each spectrum separately for a specific value of l and then form an ensemble having the same symmetry. Next in order to study the spectral fluctuation of this unfolded spectrum we utilize the following statistical tools. Nearest-neighbor spacing distribution (NNSD) is the most applied tool in the study of short-range spectral correlations. From the unfolded spectrum, we calculate the nearest-neighbor spacing as $s = E_{i+1} - E_i$ and calculate the probability distribution $P(s)$. Uncorrelated spectra obey the Poisson statistics and $P(s) = e^{-s}$. Whereas for the system with time-reversal symmetry, level repulsion leads to a Wigner-Dyson distribution $P(s) = \frac{\pi}{2} s e^{-\frac{\pi s^2}{4}}$ [39]. The Δ_3 statistics is commonly used to investigate long-range correlations. It gives a statistical measure of the rigidity of a finite spectral level sequence. For a given interval L, it is often determined by the least-square deviation of the staircase from the best straight line fit.

The $P(s)$ distribution of the unfolded energy spectrum of 1000 interacting bosons in the external trap is presented in Figs. 1(a)–1(d) [see figure caption].

For comparison Poisson statistics and GOE statistics are also given in the same figure. For the lowest 100 levels there is no level with very small spacing and no level beyond $s = 2.0$. Although the peak arises at $s \simeq 1.0$, it strongly deviates from the Wigner distribution. For such low-lying levels, the effect of interatomic interaction is dominating and levels are highly correlated. This is also intuitively right as we may write the many-body effective potential in the following way:

$$\omega_0(r) = V_{\text{trap}} + \mathcal{V}(r) = \tfrac{1}{2} m\omega^2 r^2 + \mathcal{V}(r), \qquad (19)$$

where V_{trap} is the external harmonic trap as described earlier and $\mathcal{V}(r)$ is obtained by the diagonalization of the potential matrix together with the hypercentrifugal repulsion. Now for a small value of r (which corresponds to the low-lying energy level) the effect of $\mathcal{V}(r)$ dominates. Although it was expected that these levels would exhibit a chaotic signature and follow the Wigner distribution, the level repulsion is masked due to the existence of an external harmonic trap. Thus it exhibits a mixed statistics which could not be perfectly interpolated between the Poisson and Wigner distributions by using the Brody parameter [9]. Thus the evolution of the $P(s)$ distribution clearly shows the presence of two energy scales. The situation becomes more interesting for intermediate levels. The $P(s)$ distribution for 100 to 500 levels exhibits two peaks as shown in Fig. 1(b). The first narrow peak appears at $s = 0$ with a second broad peak near $s = 1.5$. For such intermediate levels, parts of the levels are correlated and show normal level-repulsion, whereas other parts do not repel each other and try to maintain the Poisson statistics which is reflected as a first peak at $s = 0$. The effect of the level repulsion is manifested in the second peak. It is very similar to the classical mixed system, a part of the phase space is completely regular while the other part is chaotic. We have checked that by varying the number of levels in such an intermediate band, the width and peak values

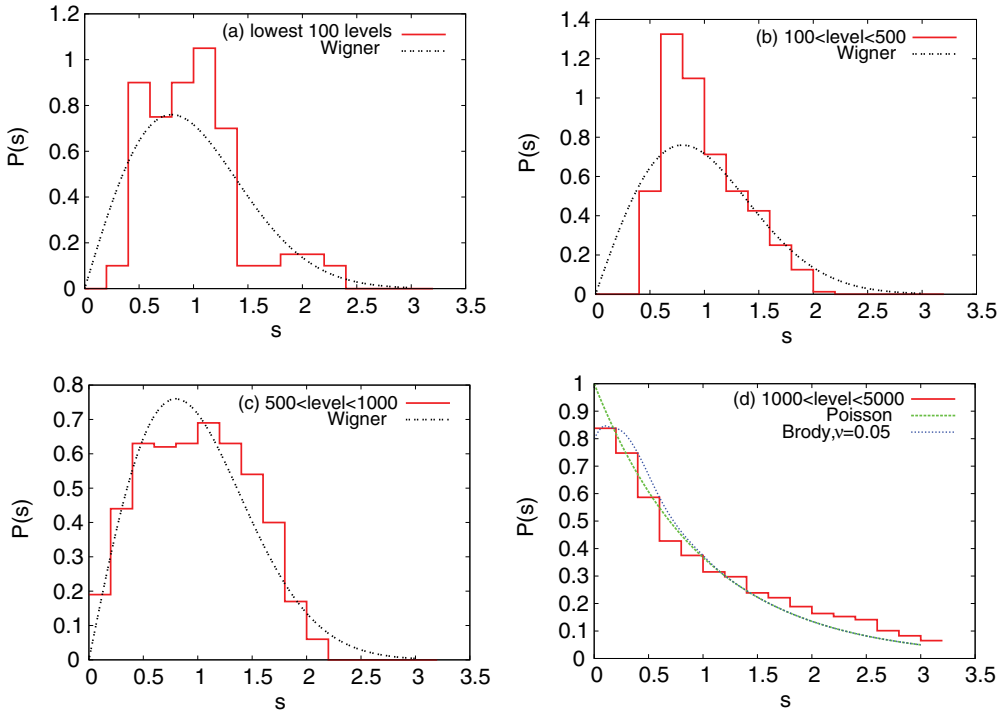

FIG. 2. (Color online) The $P(s)$ distribution is presented for different numbers of levels as indicated below the panels: (a) lowest 100 levels, (b) 100 to 500 levels, (c) 500 to 1000 levels, and (d) 1000 to 5000 levels. In each panel the histogram presents the $P(s)$ distrubution for the Hamiltonian (1) with $N = 5000$ interacting bosons. In panels (a)–(c): the black dotted curve represents the Wigner distribution. In panel (d) the green dashed curve represents the Poisson distribution while the blue dotted curve corresponds to the Brody distribution, the corresponding Brody parameter being $\nu = 0.05$.

change but qualitative features remain the same. For much higher levels, the effect of interatomic interaction gradually decreases and the effect of the harmonic trap starts to dominate. Thus more and more states are coupled in regular uncorrelated distribution. It is well reflected in Fig. 1(c), where we see that a large part of the levels tries to exhibit Poisson statistics whereas a small fraction of the levels is associated with a level repulsion, with a small peak near $s = 2.0$. For much higher levels the effect of interatomic interaction is almost negligible and the levels become regular and close to the integrable system. The $P(s)$ distribution is very close to the Poisson distribution, but the peak value at $s = 0$ is less than 1. We fit the histogram with the Brody distribution [9],

$$P(\nu,s) = (1+\nu)as^{\nu}\exp(-as^{1+\nu}), \tag{20}$$

where $a = [\Gamma(\frac{2+\nu}{1+\nu})]^{1+\nu}$ and ν is the Brody parameter. The interesting feature of this distribution is that it interpolates between the Poisson distribution ($\nu = 0$) of regular systems and the Wigner distribution with $\nu = 1$. Thus the degree of chaos is determined by the value of ν. For quantitative comparison, we fit the $P(s)$ histograms to $P(\nu,s)$ in Fig. 1(d) and the calculated repulsion parameter is $\nu = 0.04$.

The results for 5000 bosons are presented in Figs. 2(a)–2(d) [see figure caption]. As the condensate is repulsive, with an increase in particle number, the condensate wave function spreads out as the net effective repulsion Na_{sc} increases. With an increase in interaction more and more many-body levels show level repulsion and we expect level spacing distribution close to the Wigner distribution which is very similar to the completely chaotic system. But in our system as the level repulsion is suppressed by the external trap, the $P(s)$ distribution deviates from the Wigner distribution. This clearly shows the presence of two energy scales even for such intermediate levels. For 500 to 1000 levels, we see quantum chaos sets in and $P(s)$ is very close to the Wigner distribution. To observe and determine the best fit window to the Wigner distribution, the $P(s)$ distributions for 501–600, 601–700, and 701–800 levels are plotted in Fig. 3. We observe that 601–700 is the best fit window and the corresponding Brody parameter is $\nu = 0.9$. However this energy window strongly depends on the number of atoms and the scattering length, whereas for much higher levels, we observe a crossover from Wigner-like level repulsion to the Poisson distribution. In Fig. 2(d) we again compare the histogram with the Brody distribution and the corresponding Brody parameter is $\nu = 0.05$.

We observe that $P(s)$ distribution depends crucially on the number of levels and on the net effective interaction Na_{sc}. To get a more detailed physical picture we calculated the energy levels for 10 000 bosons and plotted the $P(s)$ distribution (Fig. 4). Due to strong repulsive interaction ($Na_{sc} \sim 2.09$), the low-lying levels are highly correlated and should show strong level-repulsion. In Fig. 4, we present the $P(s)$ distribution for the lowest 50 levels. Although the distribution has a sharp peak near $s = 0.8$, the distribution shows Wigner-like level repulsion. Comparing the same for 5000 bosons (Fig. 3), we observe the signature of level correlation for much lower

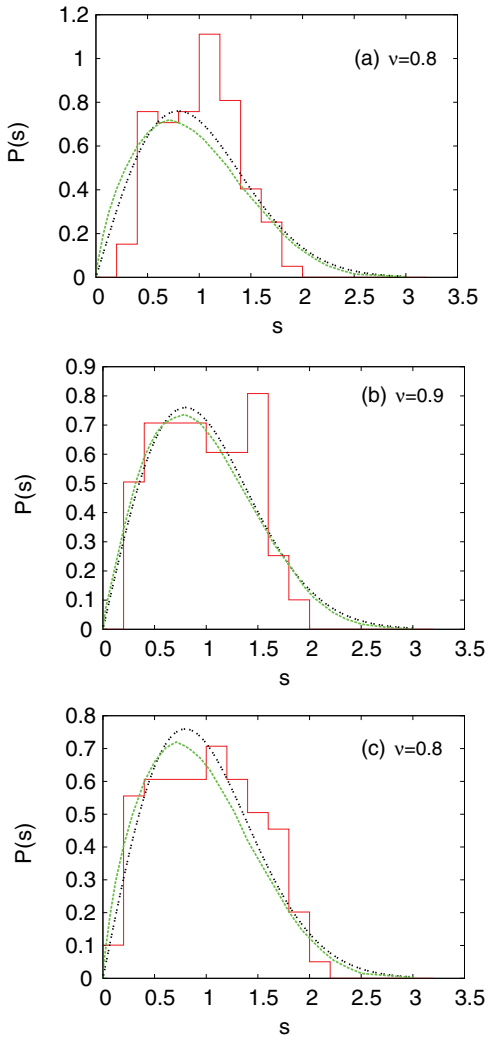

FIG. 3. (Color online) The $P(s)$ distribution is presented for different regions of the spectrum: (a) 501–600 levels, (b) 601–700 levels, and (c) 701–800 levels. In each panel the histogram presents the $P(s)$ distrubution for the Hamiltonian (1) with $N = 5000$ interacting bosons. The black dotted curve represents the Wigner distribution. The green dashed curve corresponds to the Brody distribution with the corresponding Brody parameter indicated in each panel.

levels. We also observe the uncorrelated Poisson distribution for higher levels as observed earlier.

Now in this connection it is worth calculating the spectral distribution for the energy levels which are calculated by the GP mean-field equation. As the mean-field equation uses the zero-range contact interaction and it completely ignores the interatomic correlation, it is interesting to observe the effect of finite-range interaction and interparticle correlation in the spectral statistics. For the calculation of energy levels we use the dispersion law of the discretized normal modes for the spherical trap which is given by [40]

$$\omega(n_r,l) = \omega\left(2{n_r}^2 + 2n_r l + 3n_r + l\right)^{\frac{1}{2}}. \qquad (21)$$

Here n_r is the radial quantum number and $n_r = 0$ corresponds to the surface excitation, whereas the monopole oscillation corresponds to $n_r = 1$ and $l = 0$. Note that Eq. (21) has the

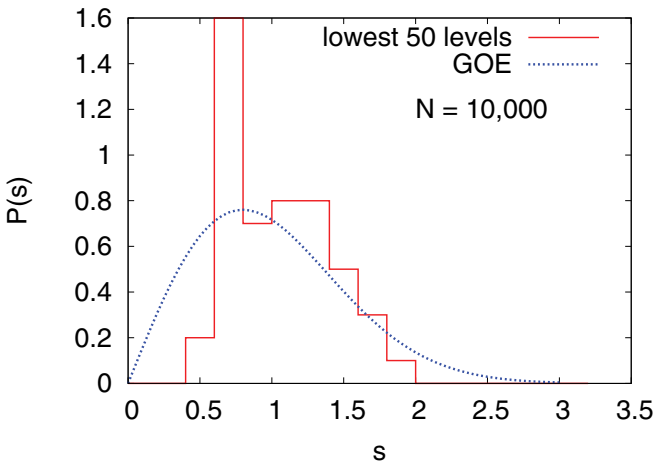

FIG. 4. (Color online) Plot of the $P(s)$ distribution for the lowest 50 levels with $N = 10\,000$ interacting bosons. The histogram represents the many-body result obtained for the Hamiltonian (1). The blue dotted curve represents the Wigner distribution.

dependence only on the radial nodes and angular momentum; azimuthal degeneracy thus exists. Equation (21) is also valid in the collisionless hydrodynamics where the number of atoms in the trap is quite high. For our chosen set, $N = 5000$ and $a_{sc} = 2.09 \times 10^{-4}$ o.u., the parameter $\frac{Na_{sc}}{a_{ho}} \simeq 1.045$, which is just greater than 1 and Eq. (21) will be valid for lower n_r and l. To see the accuracy of Eq. (21), we plot in Fig. 5(a) the ground-state energy per particle (E/N) as a function of n_r for $l = 0$. The GP results start to be lower and lower for larger n_r. The trend is maintained for other higher values of l. Our many-body results start to be higher near $n_r = 200$ due to the presence of the hypercentrifugal repulsion term in the many-body equation [Eq. (13)]. As pointed out in Ref. [40], Eq. (21) is accurate for $\hbar\omega < \mu$. Thus for the calculation of the $P(s)$ distribution using the GP results we take the lowest 500 levels for which the above condition is valid. It guarantees that our choice of levels will be reliable for the calculation of the spectral distribution. In Fig. 5(b) we plot the $P(s)$ distribution for the lowest 500 levels obtained from the dispersion law. It nicely shows the existence of a large number of quasidegenerate states as $P(s)$ exhibits a sharp peak near $s = 1$. The existence of degeneracy is also seen in Eq. (21) where the discrete eigenmode frequency $\omega(n_r,l)$ of the spatial variation of density, obtained in the context of the hydrodynamic model of the condensate at low temperature, is a function of the radial quantum number n_r and the orbital quantum number l only and hence is degenerate with respect to the azimuthal quantum number m. The contact δ potential in the GP equation cannot lift this degeneracy. There is a δ-type peak at about $s = 1$.

This behavior is again expected from Eq. (19). In the mean-field results $\mathcal{V}(r)$ is calculated taking only the contact δ interaction and ignores the interatomic correlation completely. Thus it cannot lift the degeneracy of the external harmonic trap completely. Whereas in our many-body calculation the short-range hard sphere below the cutoff radius and the $-\frac{C_6}{x^6}$ tail in the interatomic interaction takes care of the effect of both short-range correlation and long-range correlation and gives the actual physical picture. But $P(s)$ contains no information about spatial correlation. A simple measure of

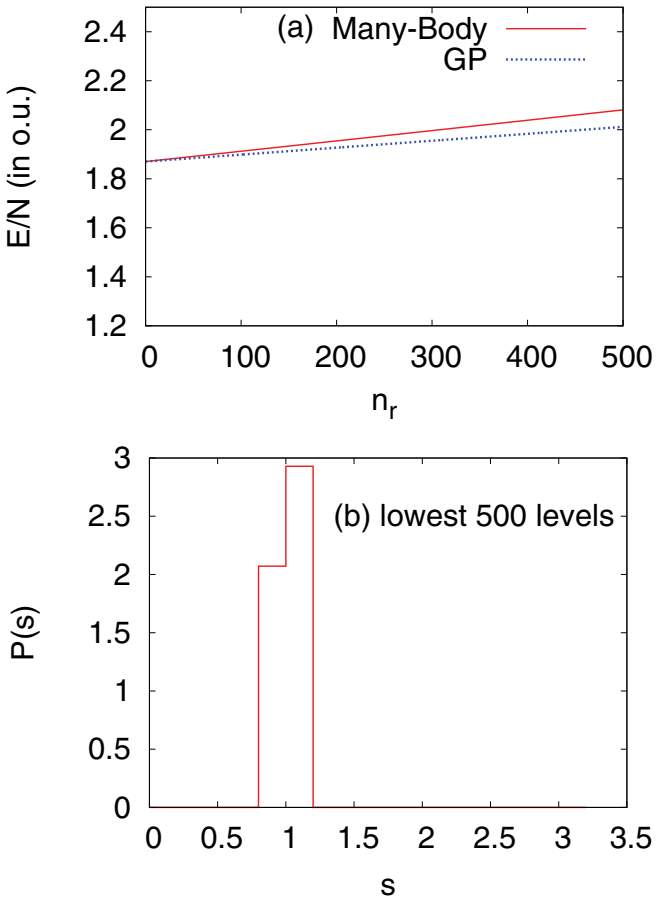

FIG. 5. (Color online) (a) Plot of the ground-state energy (in o.u.) per atom (E/N), obtained from the many-body theory and the GP theory, as a function of n_r for $l = 0$. (b) The $P(s)$ distribution obtained from the GP calculation is presented as a histogram.

spacing correlation is the correlation coefficient C defined as

$$C = \sum_i (s_i - 1)(s_{i+1} - 1) \Big/ \sum_i (s_i - 1)^2. \qquad (22)$$

For uncorrelated spectra $C = 0$. The calculated value of C for Fig. 5(b) is 1.0, which again signifies the existence of bulk quasidegenerate states.

Here we observe that the $P(s)$ distribution strongly depends on the number of energy levels and also on the net effective interatomic interaction. Thus it is hard to determine the correlation properties from only the study of the $P(s)$ distribution. It requires the study of the correlation properties in the large energy scale which will give new physical insights. The spectral rigidity is often used as a stronger tool than the level distribution in the analysis of complex systems as it can take into account the long-range correlation between the levels while the $P(s)$ distribution takes into account only nearest-neighbor correlations. Therefore further studies are needed in this direction. We are mainly interested in the Δ_3 statistics of Dyson and Mehta [41] which gives a statistical measure of the rigidity of a finite spectral level sequence. For a level sequence with a constant average level spacing, the staircase function on the average follows a straight line. Thus Δ_3 statistics gives a measure of the size of fluctuations

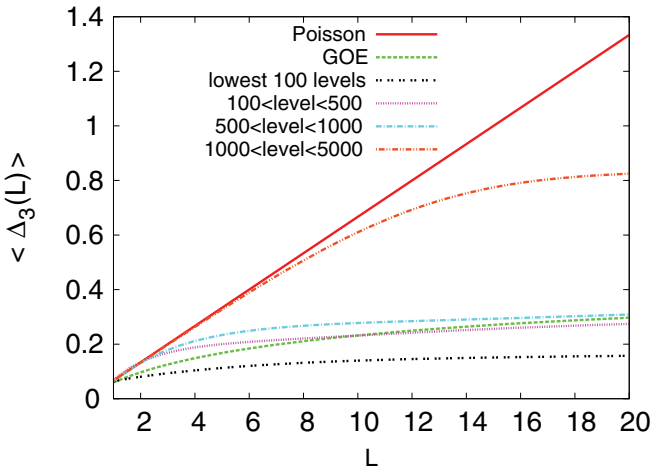

FIG. 6. (Color online) Spectral average $\langle \Delta_3(L) \rangle$ computed for the Hamiltonian (1) with $N = 1000$ interacting bosons in the external trap. The black dot-dot curve corresponds to the lowest 100 levels. The magenta dotted curve corresponds to levels between 100 and 500. The sky-blue dot-dashed curve corresponds to levels between 500 and 1000. The red broken curve corresponds to levels between 1000 and 5000. The red solid straight line corresponds to the Poisson distribution and the green dashed curve corresponds to the GOE results.

of the staircase function around a best fit straight line. For a Poisson spectrum, the levels are uncorrelated, the spectrum is rigid and $\langle \Delta_3(L) \rangle = \frac{L}{15}$, whereas for the GOE distribution, the levels are strongly correlated and $\langle \Delta_3(L) \rangle \propto \ln L$. To confirm our earlier findings of the $P(s)$ distribution we next study the correlation structure and Δ_3 statistics for our system, which are shown in Figs. 6 and 7. The results $\langle \Delta_3(L) \rangle$ are plotted against L for the same parameters and the same number of levels as chosen in Figs. 1 and 2. The results for 1000 interacting bosons are presented in Fig. 6. For comparison we also plot $\langle \Delta_3(L) \rangle$ for the Poisson and the GOE prediction. For low-energy levels we observe the same trend, bending toward the GOE prediction. However the saturated value is well below the GOE prediction. It again reflects the fact that level repulsion due to interatomic interaction is screened due to the effect of the external harmonic trap. For 1000–5000 levels, $\langle \Delta_3(L) \rangle$ follows the expected straight line behavior up to $L \leqslant 10$, which is the result of integrable systems. But beyond $L = 10$, it still tends to saturation, but it is consistent with Berry's semiclassical arguments [42,43].

The results for 5000 bosons are shown in Fig. 7, which again indicates that lower levels are highly correlated whereas for higher levels we get the signature of more regular distribution.

It is useful to mention that Guhr and Weidenmüller [44] studied in the past the spectral properties of a regular Hamiltonain perturbed by a GOE. The results for 100 levels and 100 to 500 levels shown in the present work are quite similar to some of the results in Figs. 1, 2, 3, and 6 of Ref. [44] where a modified uniform spectrum was used as the regular Hamiltonian. Therefore, a quantitative description of the results in Figs. 1–5 in terms of a deformed GOE, which combines uniform, GOE, and Poisson results is possible but this is for a future investigation. This variety of behavior has also been observed early in the study of quantum mechanics of

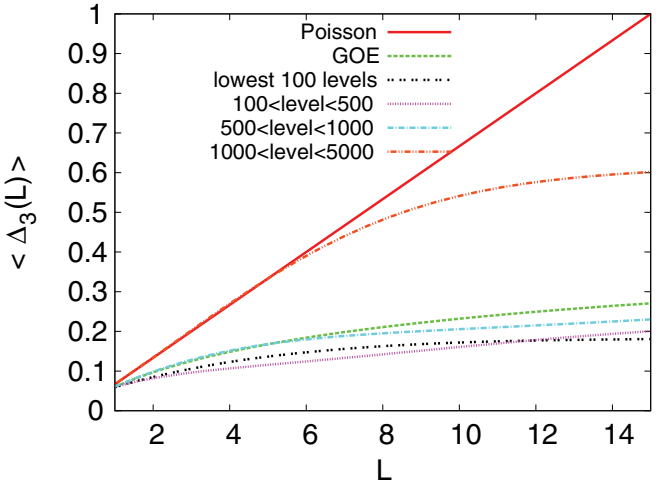

FIG. 7. (Color online) Spectral average $\langle \Delta_3(L) \rangle$ computed for the Hamiltonian (1) with $N = 5000$ interacting bosons in the external trap. The black dot-dot curve corresponds to the lowest 100 levels. The magenta dotted curve corresponds to levels between 100 and 500. The sky-blue dot-dashed curve corresponds to levels between 500 and 1000. The red broken curve corresponds to levels between 1000 and 5000. The red solid straight line corresponds to the Poisson distribution and the green dashed curve corresponds to the GOE results.

heavier clusters like Kr and Xe trimers. The energy spectra of these clusters show a wide variety of behavior below and above the transition energy [45]. Very regular behavior of low-lying eigenstates changes to the combination of regular and irregular behavior at energy above the transition energy.

Experiments on BEC with ^{7}Li atoms is another challenging research area where the s-wave scattering length (a_s) is negative, which indicates that atom-atom interaction is negative [46]. A homogeneous condensate with a negative scattering length is impossible as the condensate approaches collapse. However the situation changes drastically in the presence of an external confinement. Spatially confined BEC is stable for a small, finite number of atoms ($N_{\rm cr}$). For ^{7}Li, $a_s = -27.3$ bohrs $= -45.7 \times 10^{-5}$ o.u. and for $T = 0$ a metastable condensate exists when the number of atoms is less than the critical number $\simeq 1300$ [47], whereas theory predicts that BEC can occur in a trap with no more than about 1400 atoms [48].

It has been pointed out earlier in a different context [49,50] that the GP theory based on the pseudopotential form of the interatomic interaction is not suitable as an exact potential in a three-dimensional attractive system. Again as the attractive BEC becomes highly correlated near the critical points, the uncorrelated GP equation cannot take care of the effect of the interatomic correlation. In our earlier calculation we have extensively applied our many-body method in the study of different properties and of the stability of the attractive condensate [51,52]. In our present study we are interested in the spectral distribution of highly correlated BEC. The presence of a hard sphere below some cutoff radius and the $-\frac{C_6}{x^6}$ tail in the interatomic interaction properly takes care of the effect of both short-range and long-range correlations.

For $N < N_{\rm cr}$, the condensate is metastable. In the many-body effective potential, the intermediate metastable region

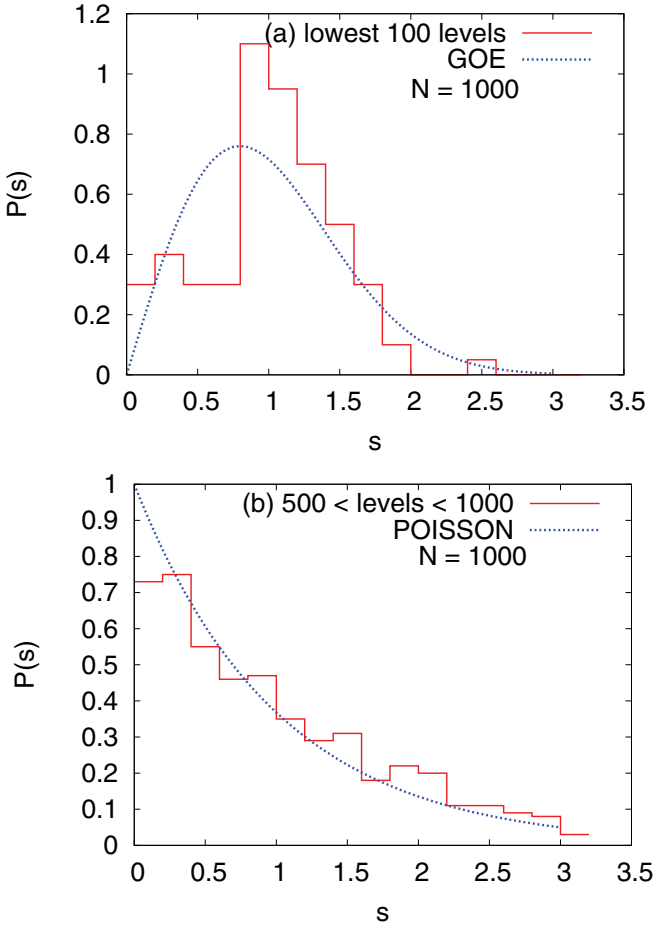

FIG. 8. (Color online) Plot of the $P(s)$ distribution for different numbers of levels in different regions of spectra of $N = 1000$ ^{7}Li atoms. In each panel the histogram presents the $P(s)$ distribution obtained from the many-body theory. In panel (a) the blue dotted curve corresponds to the Wigner (GOE) distribution, and in panel (b) it corresponds to the Poisson distribution.

(MSR) is bounded by the high wall of the external trap on the right side and a very deep narrow attractive well appears on the left side of the left intermediate barrier [52]. As the very high-lying levels will have a large probability of tunneling through the barrier we are interested only in the low-lying levels for which the transition probability is almost zero. The results for $N = 1000$ and $N = 1300$ are presented in Figs. 8 and 9, respectively. We do not get any stable solution beyond $N = 1320$. So for our present calculation the critical number is $N_{\rm cr} = 1320$. For $N = 1000$, as the number of atoms is well below the critical number, we correctly obtain the lowest 100 levels, which are well contained within the metastable region. We observe high level-correlation for the lowest 100 levels and the high-lying levels are uncorrelated. The effect of interatomic correlation for attractive BEC is very important for low-lying levels as the effect of $\mathcal{V}(r)$ dominates for smaller values of r. Although the level correlation strongly dominates, we do not observe any δ-function-like peak. This signifies that for $N = 1000$, the exact degeneracy of the harmonic oscillator is completely removed by the interatomic interaction $\mathcal{V}(r)$, whereas for larger r, as the term $\frac{1}{2}m\omega^2 r^2$ dominates we get the uncorrelated Poisson distribution. The

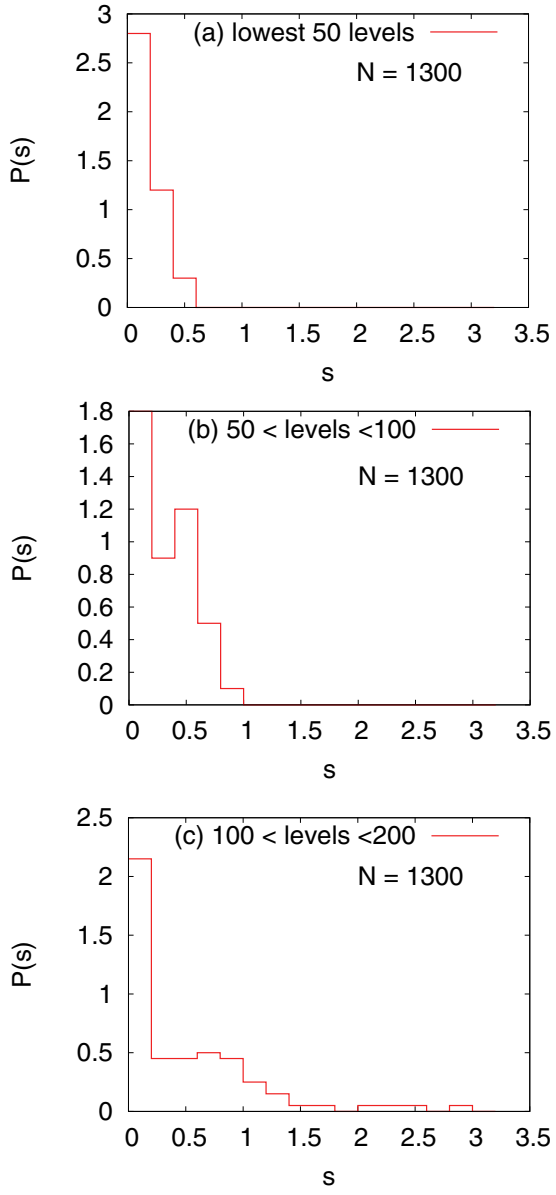

FIG. 9. (Color online) The $P(s)$ distribution for different numbers of levels of $N = 1300$ ^{7}Li atoms in the trap is presented as a histogram. Panel (a) corresponds to the lowest 50 levels, panel (b) corresponds to the lowest 50–100 levels, and panel (c) corresponds to the lowest 100–200 levels as indicated in each panel.

situation becomes more interesting for $N = 1300$ which is very close to the critical point and the condensate is highly correlated. This is reflected in Figs. 9(a)–9(c) where we plot $P(s)$ for different levels. Because near the critical point the metastable region becomes flatter, we calculate the lowest 200 levels for which the tunneling probability through the intermediate barrier is negligible. For the lowest 50 levels [Fig. 9(a)] we observe a sharp peak in the first bin near $s = 0$. It signifies that many eigenstates overlap and it leads to the existence of large quasidegenerate states. Such a δ-type peak in the $P(s)$ distribution is called a Shnirelman peak [53,54]. In the year 1993, Shnirelman showed that systems with time-reversal symmetry should exhibit the Shnirelman peak in the $P(s)$ distribution. This peak appears due to the presence of symmetry, and separating levels by symmetry, one will get back the Poisson distribution. This indicates the presence of bulk quasidegenerate states in the level spacing distribution. In the first verification of the Shnirelman theorem, Chirikov and Shepelyansky [54] studied the kicked rotator on a torus with time-reversal symmetry. Later the theorem was verified in a more real physical quantum system [55]. Very recently we have also observed the Shnirelman peak in the level spacing distribution for three interacting bosons in the external harmonic trap [56]. In the noninteracting limit, the external trap should exhibit the exact degeneracy; however, due to the presence of a small two-body interaction in the three-boson system, the exact degeneracy is removed and the quasidegeneracy is left. This is also clear from Eq. (19) where $\mathcal{V}(r)$ still dominates and the continuous symmetry of the harmonic oscillator is removed, but discrete symmetry is retained. In Figs. 9(b) and 9(c), although we get a sharp peak near $s = 0$, it spreads to further bins. This signifies that the effect of quasidegeneracy is gradually lifted at the higher levels.

V. CONCLUDING REMARKS

Using the correlated many-body technique we compute the energy spectrum of weakly interacting trapped Bose gas. All throughout our calculation the Bose gas is at zero temperature and under harmonic confinement with a fixed trap size which corresponds to the JILA experiment. Although the statistical behavior of completely integrable and fully chaotic systems are understood, the intermediate region of integrability and chaos is more interesting. Interacting trapped bosons are such a system which is spatially inhomogeneous. The existence of an external harmonic trap together with interatomic interaction makes the system more interesting. We study the spectral fluctuation and level correlation in the energy spectrum. Although there is no rigorous derivation, the numerical results show a mixed statistics, which is complexly dependent on the number of energy levels and the number of the bosons in the trap. However for higher energy levels where the external trap is dominating we get back the Poisson type fluctuation, whereas the low-lying collective excitations are strongly influenced by interatomic interaction and show level repulsion. Thus our findings do not strictly obey the earlier conjecture of Bohigas *et al.* [2] for atomic nuclei and atoms. The results for attractive Bose gas near the critical point is highly interesting and nicely show how the degeneracy of the harmonic trap is gradually removed for the higher levels. Although there are no experimental data for such high-lying states, for dilute interacting Bose gas it is possible to measure them experimentally with present-day setups. Our present study opens many questions for further study. In the present study the interacting Bose gas is in a fixed trap size. However the use of time-dependent potentials will allow the study of the dynamical behavior of energy spectra and the time evolution of the spectral statistics and correlation properties. Throughout our calculation we use the zero-temperature Bose gas and deliberately avoid any thermal fluctuations. Therefore it is also interesting to study the spectral distribution for nonzero-temperature BEC. Our present methodology is not valid as it avoids the thermal fluctuation.

ACKNOWLEDGMENTS

We thank Professor Luca Salasnich for fruitful discussions. This work is supported in part by the DAE (Grant No. 2009/37/23/BRNS/1903) and the DST [Fund No. SR/S2/CMP/0059(2007)]. AB acknowledges the Council of Scientific and Industrial Research (CSIR), India, for a senior research fellowship [Grant No. 09/028(0773)-2010-EMR-1]. SKH also acknowledges the CSIR, India, for a junior research fellowship (Grant No. 08/561(0001)/2010-EMR-1).

[1] M. V. Berry and M. Tabor, Proc. R. Soc. London A **356**, 375 (1977).
[2] O. Bohigas, M. J. Giannoni, and C. Schmit, Phys. Rev. Lett. **52**, 1 (1984).
[3] G. Casati, F. Valz-Gris, and I. Guarneri, Lett. Nuovo Cimento Soc. Ital. Fis. **28**, 279 (1980).
[4] F. Haake, *Quantum Signatures of Chaos* (Springer, New York, 2010).
[5] T. H. Seligman, J. J. M. Verbaarschot, and M. R. Zirnbauer, Phys. Rev. Lett. **53**, 215 (1984).
[6] T. Zimmermann, H.-D. Meyer, H. Köppel, and L. S. Cederbaum, Phys. Rev. A **33**, 4334 (1986).
[7] G. Tanner, K. Richter, and J.-M. Rost, Rev. Mod. Phys. **72**, 497 (2000).
[8] J. Sakhr and N. D. Whelan, Phys. Rev. A **62**, 042109 (2000).
[9] T. A. Brody *et al*., Rev. Mod. Phys. **53**, 385 (1981).
[10] V. K. B. Kota, Phys. Rep. **347**, 223 (2001).
[11] J. M. G. Gómez, K. Kar, V. K. B. Kota, R. A. Molina, A. Relaño, and J. Retamosa, Phys. Rep. **499**, 103 (2011).
[12] L. Muñoz, E. Faleiro, R. A. Molina, A. Relano, and J. Retamosa, Phys. Rev. E **73**, 036202 (2006).
[13] R. J. Leclair, R. U. Haq, V. K. B. Kota, and N. D. Chavda, Phys. Lett. A **372**, 4373 (2008).
[14] N. D. Chavda, V. Potbhare, and V. K. B. Kota, Phys. Lett. A **311**, 331 (2003).
[15] M. Vyas, N. D. Chavda, V. K. B. Kota, and V. Potbhare, arXiv:1010.6054 (cond-mat. stat-mech).
[16] M. H. Anderson *et al*., Science **269**, 198 (1995).
[17] F. Dalfovo, S. Giorgini, L. P. Pitaevskii, and S. Stringari, Rev. Mod. Phys. **71**, 463 (1999).
[18] D. S. Jin, J. R. Ensher, M. R. Matthews, C. E. Wieman, and E. A. Cornell, Phys. Rev. Lett. **77**, 420 (1996).
[19] F. Dalfovo, S. Giorgini, M. Guilleumas, L. Pitaevskii, and S. Stringari, Phys. Rev. A **56**, 3840 (1997).
[20] T. K. Das and B. Chakrabarti, Phys. Rev. A **70**, 063601 (2004).
[21] T. K. Das, S. Canuto, A. Kundu, and B. Chakrabarti, Phys. Rev. A **75**, 042705 (2007).
[22] T. K. Das, A. Kundu, S. Canuto, B. Chakrabarti, Phys. Lett. A **373**, 258 (2009).
[23] J. L. Ballot and M. Fabre de la Ripelle, Ann. Phys. (NY) **127**, 62 (1980).
[24] T. K. Das, H. T. Coelho, and M. Fabre de la Ripelle, Phys. Rev. C **26**, 2281 (1982).
[25] A. Biswas and T. K. Das, J. Phys. B **41**, 231001 (2008).
[26] B. Chakrabarti, T. K. Das, and P. K. Debnath, J. Low Temp. Phys. **157**, 527 (2009).
[27] S. Geltman, Chem. Phys. Lett. **418**, 163 (2006).
[28] B. Gao, J. Phys. B **36**, 2111 (2003).
[29] S. Geltman, Phys. Lett. A **356**, 431 (2006).
[30] B. D. Esry and C. H. Greene, Phys. Rev. A **60**, 1451 (1999).
[31] B. Chakrabarti and T. K. Das, Phys. Rev. A **78**, 063608 (2008).
[32] A. Biswas, J. Phys. B **42**, 215302 (2009).
[33] A. Biswas, T. K. Das, L. Salasnich, and B. Chakrabarti, Phys. Rev. A **82**, 043607 (2010).
[34] P. K. Debnath and B. Chakrabarti, Phys. Rev. A **82**, 043614 (2010).
[35] S. K. Haldar, B. Chakrabarti, and T. K. Das, Phys. Rev. A **82**, 043616 (2010).
[36] D. S. Jin, M. R. Matthews, J. R. Ensher, C. E. Wieman, and E. A. Cornell, Phys. Rev. Lett. **78**, 764 (1997).
[37] D. M. Stamper-Kurn, H. J. Miesner, S. Inouye, M. R. Andrews, and W. Ketterle, Phys. Rev. Lett. **81**, 500 (1998).
[38] J. R. Huzenga and L. G. Moretto, Annu. Rev. Nucl. Sci. **22**, 427 (1972).
[39] O. Bohigas and M.-J. Giannoni, in *Mathematical and Computational Methods in Nuclear Physics*, edited by J. S. Dehesa, J. M. G. Gomez, and A. Polls, Vol. 209 of Lecture Notes in Physics (Springer, New York, 1984).
[40] S. Stringari, Phys. Rev. Lett. **77**, 2360 (1996).
[41] M. L. Mehta, *Random Matrices* (Academic Press, New York, 1991).
[42] S. Droźdź and J. Speth, Phys. Rev. Lett. **67**, 529 (1991).
[43] M. V. Berry, Proc. R. Soc. London A **400**, 229 (1985).
[44] T. A. Guhr and H. A. Weidenmüller, Ann. Phys. (NY) **193**, 472 (1989).
[45] D. M. Leitner, J. D. Doll, and R. M. Whitnell, J. Chem. Phys. **94**, 6644 (1991).
[46] C. C. Bradley, C. A. Sackett, J. J. Tollett, and R. G. Hulet, Phys. Rev. Lett. **75**, 1687 (1995).
[47] C. C. Bradley, C. A. Sackett, and R. G. Hulet, Phys. Rev. Lett. **78**, 985 (1997).
[48] Y. Kagan, G. V. Shlyapnikov, and J. T. M. Walraven, Phys. Rev. Lett. **76**, 2670 (1996).
[49] S. Geltman, J. Phys. B **37**, 315 (2004).
[50] B. D. Esry and C. H. Greene, Phys. Rev. A **60**, 1451 (1999).
[51] T. K. Das, A. Kundu, S. Canuto, and B. Chakrabarti, Phys. Lett. A **373**, 258 (2009).
[52] A. Biswas, T. K. Das, L. Salasnich, and B. Chakrabarti, Phys. Rev. A **82**, 043607 (2010).
[53] A. I. Shnirelman. Usp. Mat. Nauk **30**, 265 (1975); A. I. Shnirelman, addendum in V. F. Lazutkin, *KAM Theory and Semiclassical Approximations to Eigenfunctions* (Springer, Berlin, 1993).
[54] B. V. Chirikov and D. L. Shepelyansky, Phys. Rev. Lett. **74**, 518 (1995).
[55] B. Chakrabarti and B. Hu, Phys. Rev. E **65**, 067103 (2002).
[56] K. Roy, B. Chakrabarti, A. Biswas, V. K. B. Kota, and S. K. Haldar, Phys. Rev. E **85**, 061119 (2012).